SECTION -D-

ABSOLUTE TIME CONSTRAINTS ON DEFORMATION AND ACCOMPANYING METAMORPHISM FROM IN-SITU ELECTRON MICROPROBE DATING OF MONAZITE IN THE ROBERTSON RIVER METAMORPHICS, NE AUSTRALIA

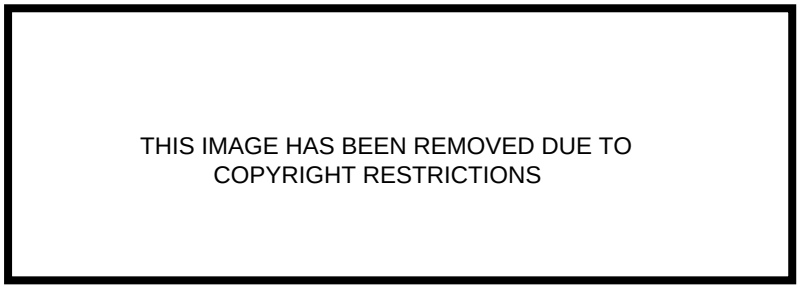

Figure 1. Location map showing major regional geological features and the area in which detailed work was done outlined by a box (Compiled from Withnall 1985).

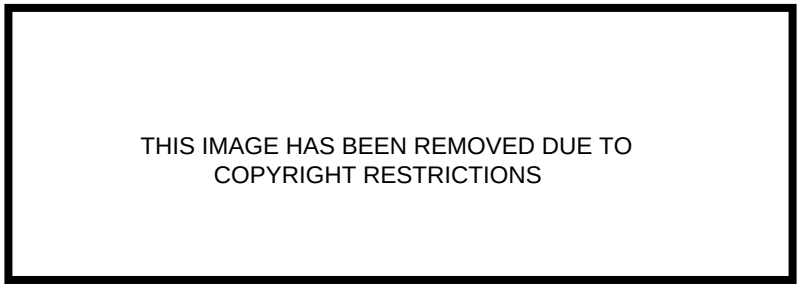
THIS IMAGE HAS BEEN REMOVED DUE TO
COPYRIGHT RESTRICTIONS

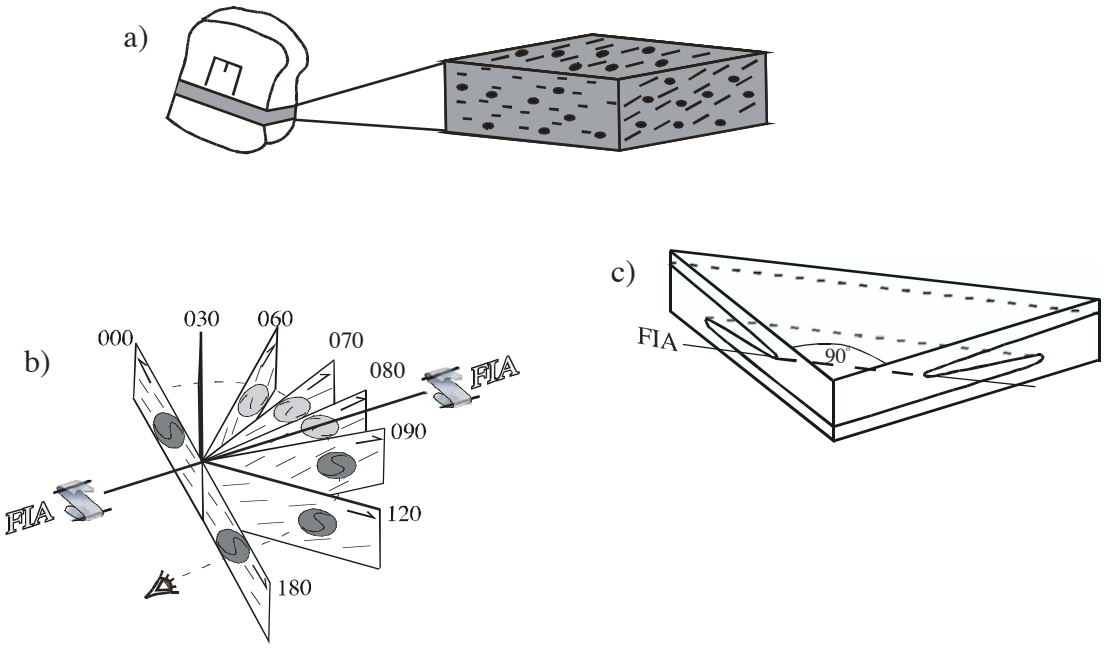

Figure 3. a) Sketches of the oriented rock sample marked and cut into a horizontal slab, from which b) multiple-vertical thin sections are cut from a horizontal rock slab. The FIA (foliation intersection/inflection axis preserved within porphyroblasts) is determined where the asymmetry of the inclusion trails changes c) when viewed from one direction.

Figure 4. Photomicrographs showing the structural features and their interpretations, observed in the matrix and within porphyroblasts; a) garnet (Grt) porphyroblast with sigmoidal type inclusion trails representing pre-S_1, wrapped by andalusite (And) overgrowing S_1, that continues through to main foliation $S_{1/2}$, and sillimanite (Sill) plus biotite (Bt) overprinting early phases; b) staurolite (St) porphyroblast replaced by andalusite in the matrix with S_1 preserved as a crenulation hinge within the staurolite and $S_{1/2}$ as the predominant foliation; c) andalusite replacing an older staurolite generation that overgrew S_1, and younger staurolite generation overgrew $S_{1/2}$. S_3 and S_4 represent a crenulated foliation and steep cleavage respectively; d) garnet porphyroblast containing staircase inclusion trails, truncated by the matrix foliations. S_2 is preserved in the strain shadow of the garnet and away from the porphyroblast it decrenulates and rotate towards $S_{1/2}$ that is overprinted by S_3; e) staurolite porphyroblast overgrew $S_{1/2}$, S_2 preserved within the porphyroblast as the steep crenulation cleavage was destroyed in the matrix because of the reactivation; f) textural relationship showing the replacement of staurolite by prograde muscovite and the overprinting of garnet and andalusite by sillimanite plus biotite. The plates at left lower corners of photos show the sample number and vertical thin section directions around compass.

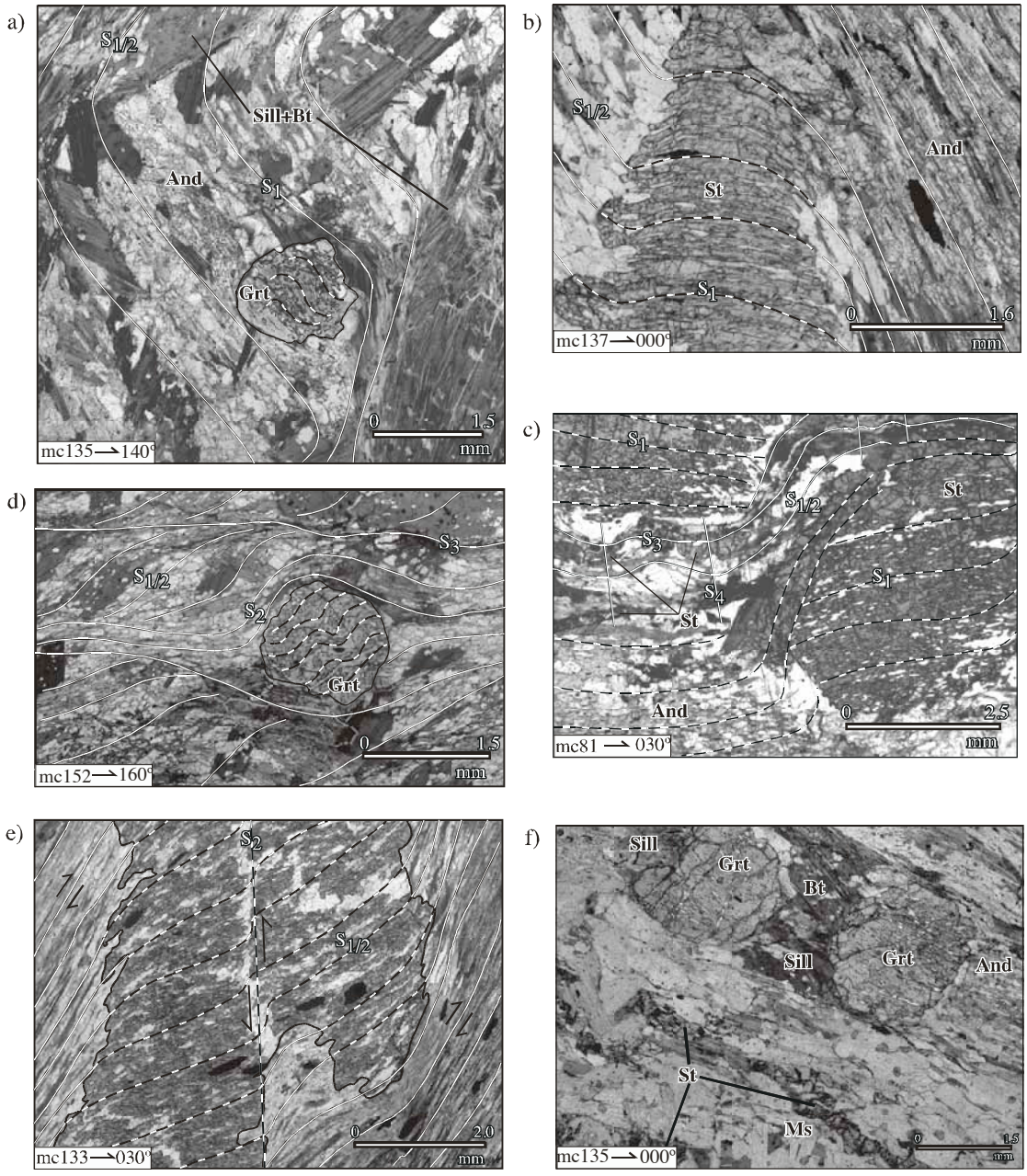
a)
S1/2
Sill+Bt
And
S1
Grt
0
1.5
mm
mc135→140°
b)
S1/2
And
St
S1
0
1.6
mm
mc137→000°
c)
S1
St
S1/2
S3
S1
S4
St
And
0
2.5
mm
mc81 → 030°
d)
S3
S1/2
S2
Grt
0
1.5
mm
mc152→160°
e)
S2
S1/2
Z
Z
0
2.0
mm
mc133→030°
f)
Sill
Grt
Bt
Sill
Grt
And
St
Ms
0
1.5
mm
mc135→000°

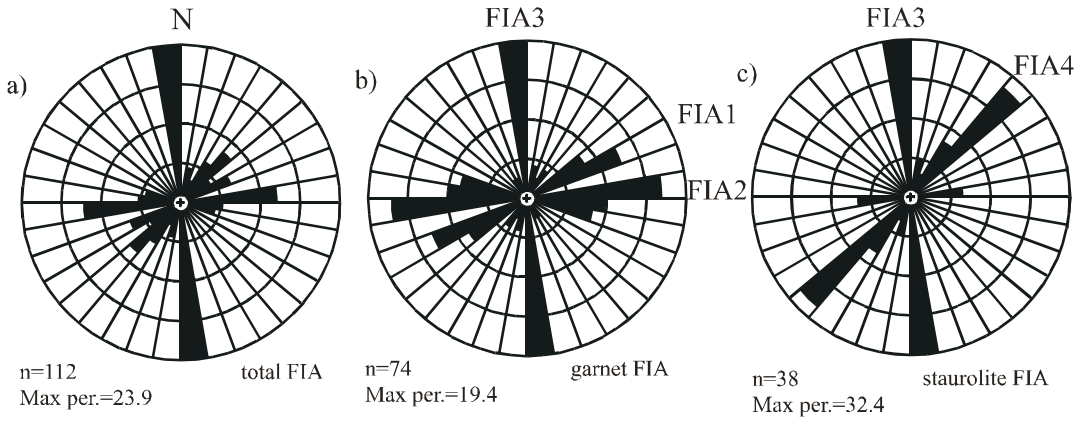

Figure 5. a) Rose diagrams showing the orientations of total FIAs, b) FIA1 (ENE-WSW), FIA2 (E-W) and FIA3 (N-S) in garnet porphyroblasts, and c) FIA2 (E-W), FIA3 (N-S) and FIA4 (NE-SW) in staurolite porphyroblasts across the study area. See Table 1 for the FIA data.

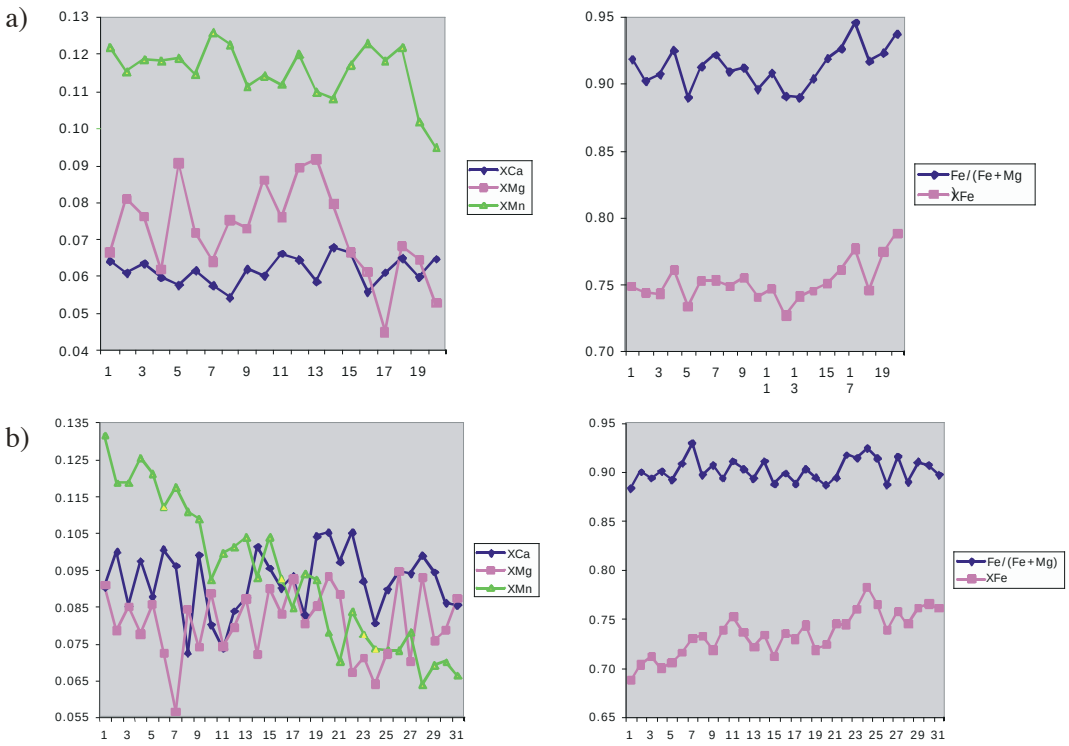

Figure 6. Compositional zoning profiles (X_{Mn}, X_{Ca}, X_{Mg}, X_{Fe} and $X_{Fe/(Fe+Mg)}$) of garnet porphyroblasts in sample mc135 (a) and mc 137 (b). In mc135 the garnet shows a lack of zoning as indicated by a flattened X_{Mn} profile, whereas in mc137 the garnet preserves growth zoning.

Figure 7. Pseudosection (a) displaying the mineral stability fields, with respect to the bulk composition of mc137 (core-gr1 in (c)). The isopleths of X_{Mn}, X_{Ca} and X_{Fe} (b) derived from the probe analysis of the core and median of a garnet are calculated and then plotted based on the compositions (c) estimated using the fractionation method of Evans (2004).

a)

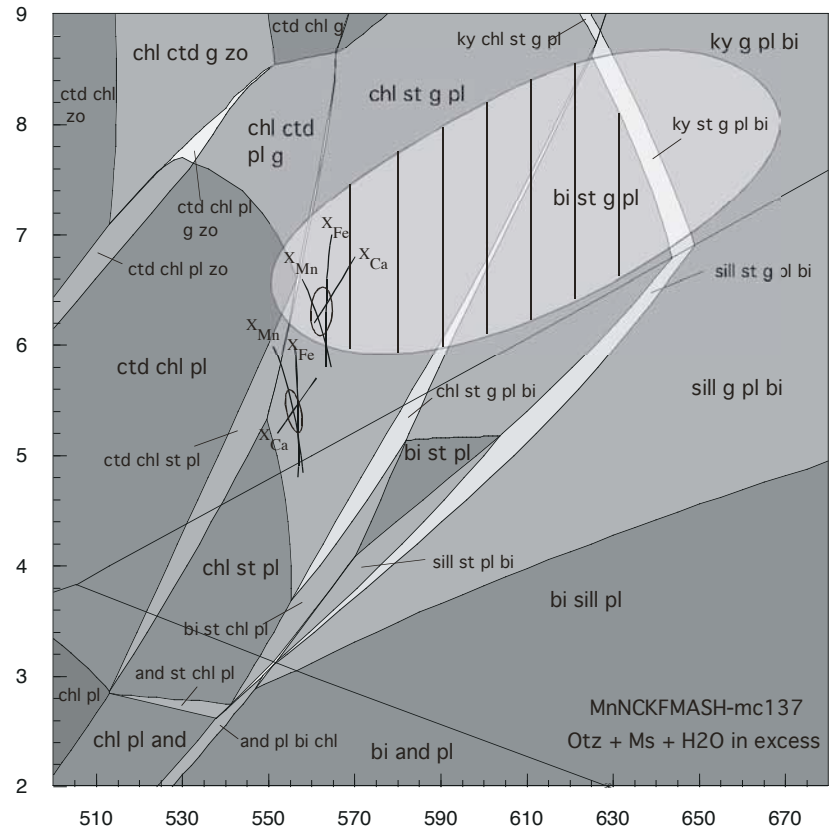

b)

	X_{Fe}	2 sigma	X_{Ca}	2 sigma	X_{Mn}	2 sigma
Core (gr1)	0.6875	0.0247	0.0901	0.0079	0.1314	0.0107
Median (gr20)	0.7238	0.0249	0.1051	0.0077	0.0779	0.0095

Bulk Rock Compositions (mol proportions; SiO_2 free)

c)

	Core (gr1)	Median(gr20)
Al_2O_3	47.66	48.16
FeO	21.24	20.51
MnO	0.40	0.24
MgO	14.53	14.71
CaO	2.94	2.85
Na_2O	4.91	5.01
K_2O	8.33	8.51
SUM	100.00	100.00

Figure 8. Backscatter images show the monazite grains and also their locations (a-e) from sample mc152. The numbered circular spots represent the locations of analyses presented in Table 4.

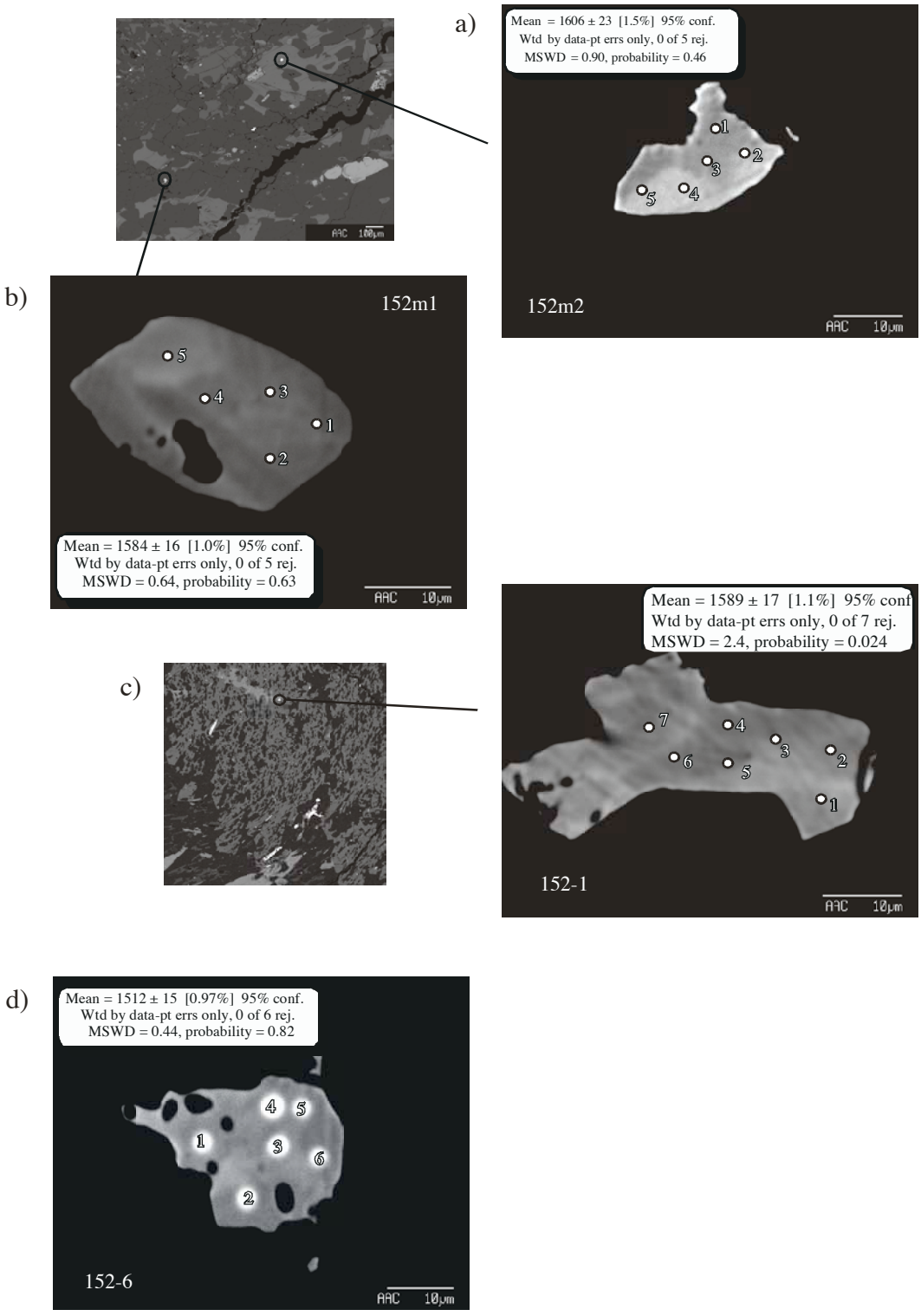
a)
Mean = 1606 ± 23 [1.5%] 95% conf.
Wtd by data-pt errs only, 0 of 5 rej.
MSWD = 0.90, probability = 0.46
152m2
AAC 10µm
b)
152m1
Mean = 1584 ± 16 [1.0%] 95% conf.
Wtd by data-pt errs only, 0 of 5 rej.
MSWD = 0.64, probability = 0.63
AAC 10µm
c)
Mean = 1589 ± 17 [1.1%] 95% conf
Wtd by data-pt errs only, 0 of 7 rej.
MSWD = 2.4, probability = 0.024
152-1
AAC 10µm
d)
Mean = 1512 ± 15 [0.97%] 95% conf.
Wtd by data-pt errs only, 0 of 6 rej.
MSWD = 0.44, probability = 0.82
152-6
AAC 10µm

Figure 9. a) Weighted average plot of 9 individual monazite ages with 95% confidence level for rock sample mc152 ; b) Probability density curve suggests three distinct age populations.

a)

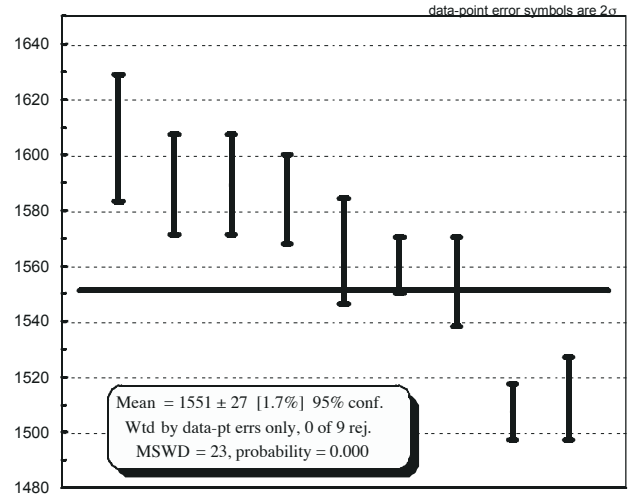

b)

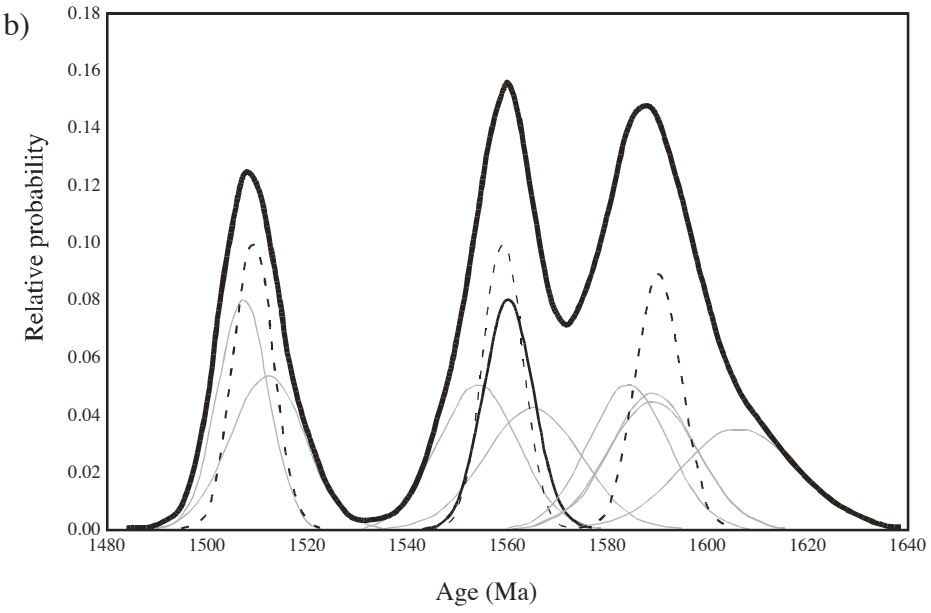

Age	±2 σ	fraction	±2 σ
1508.5	8.3	0.22	0.31
1559.5	7.9	0.33	0.39
1589.8	9.5	0.45	---

relative misfit = 0.318

Figure 10. Backscatter images show the monazite grains and also their locations (a-b) from sample mc135. The numbered circular spots represent the locations of analyses presented in Table 4.

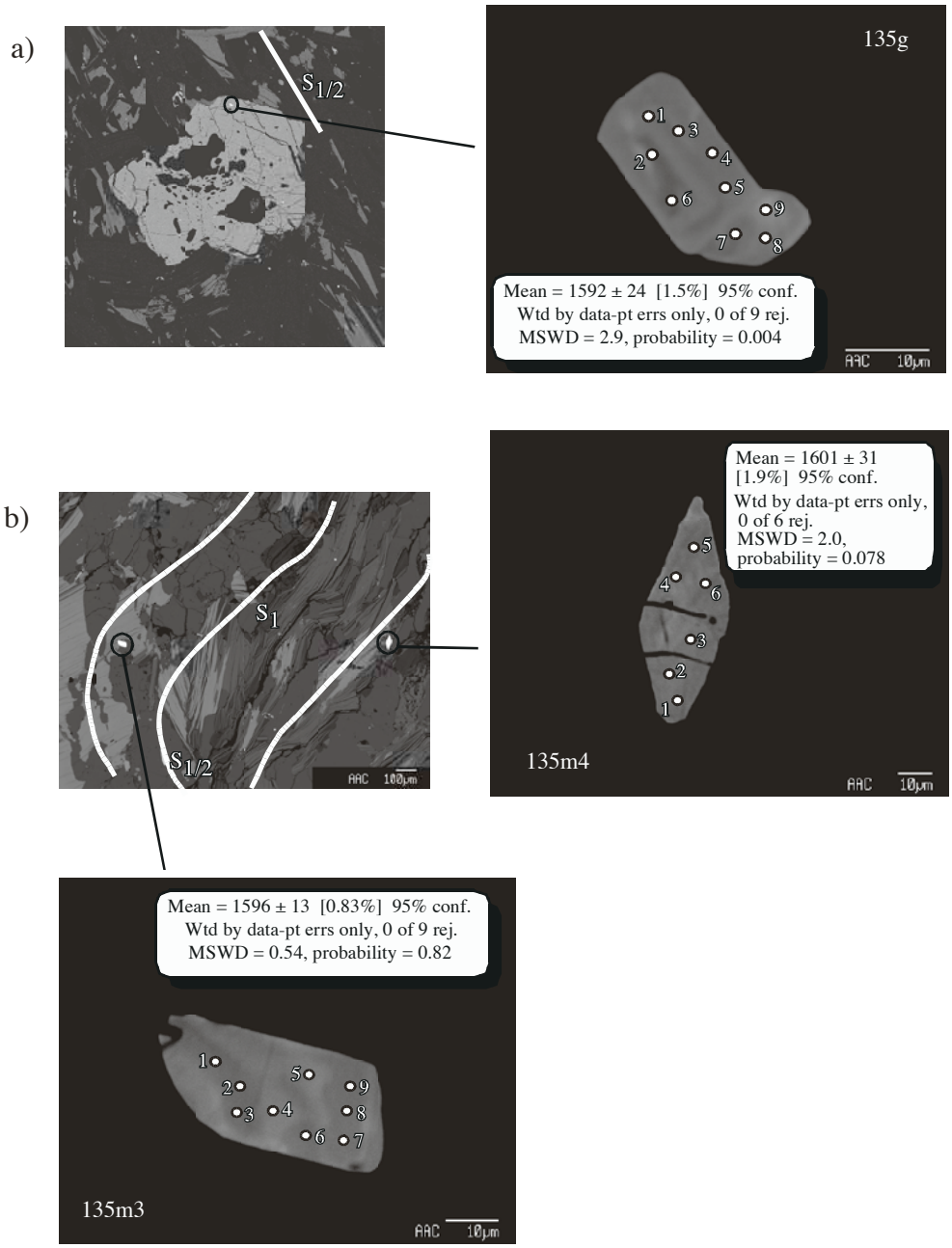
a)
S1/2
135g
1
3
2
4
5
6
9
7
8
Mean = 1592 ± 24 [1.5%] 95% conf.
Wtd by data-pt errs only, 0 of 9 rej.
MSWD = 2.9, probability = 0.004
AAC 10µm
b)
S1
S1/2
AAC 100µm
Mean = 1601 ± 31
[1.9%] 95% conf.
Wtd by data-pt errs only,
0 of 6 rej.
MSWD = 2.0,
probability = 0.078
5
4
6
3
2
1
135m4
AAC 10µm
Mean = 1596 ± 13 [0.83%] 95% conf.
Wtd by data-pt errs only, 0 of 9 rej.
MSWD = 0.54, probability = 0.82
1
5
2
9
3
4
8
6
7
135m3
AAC 10µm

Figure 11. a) Weighted average plot of 6 individual monazite ages with 95% confidence level for rock sample mc135; b) Probability density curve suggests two distinct age populations.

a)

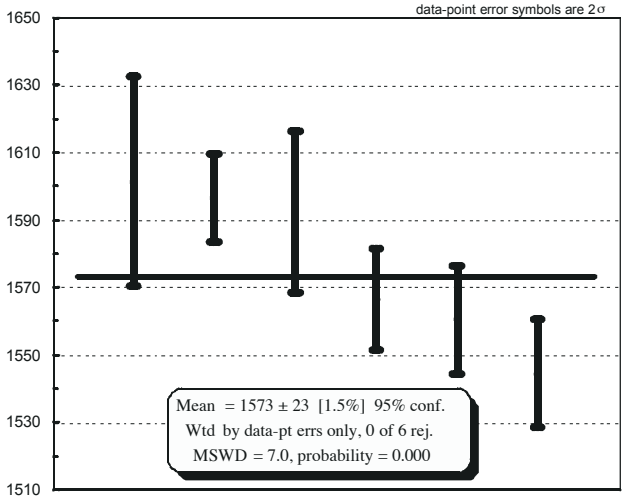

b)

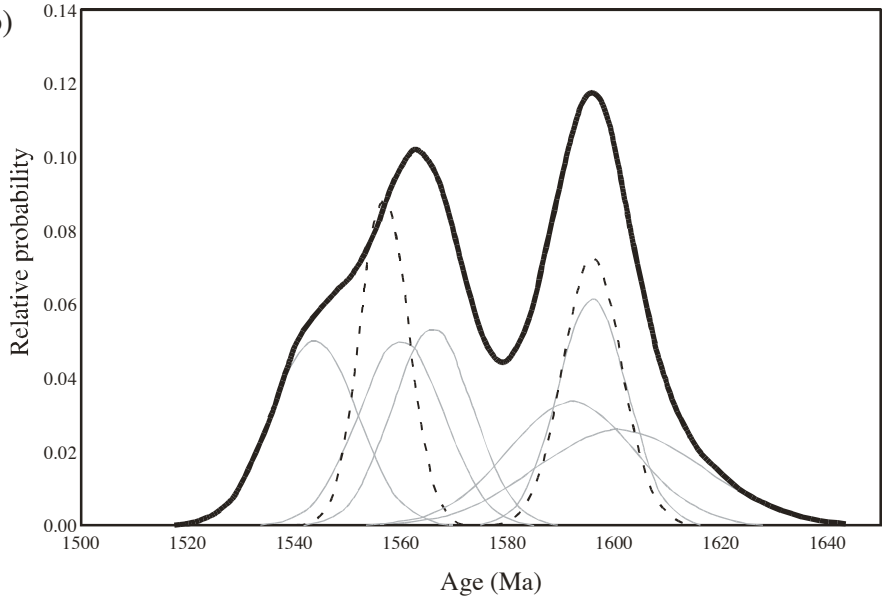

Age	±2 σ	fraction	±2 σ
1557.2	9.2	0.51	0.58
1595.8	11	0.49	---

relative misfit = 0.693

Figure 12. Backscatter electron images show the monazite grains and also their locations (a-d) from sample mc137. The numbered circular spots represent the locations of analyses presented in Table 4.

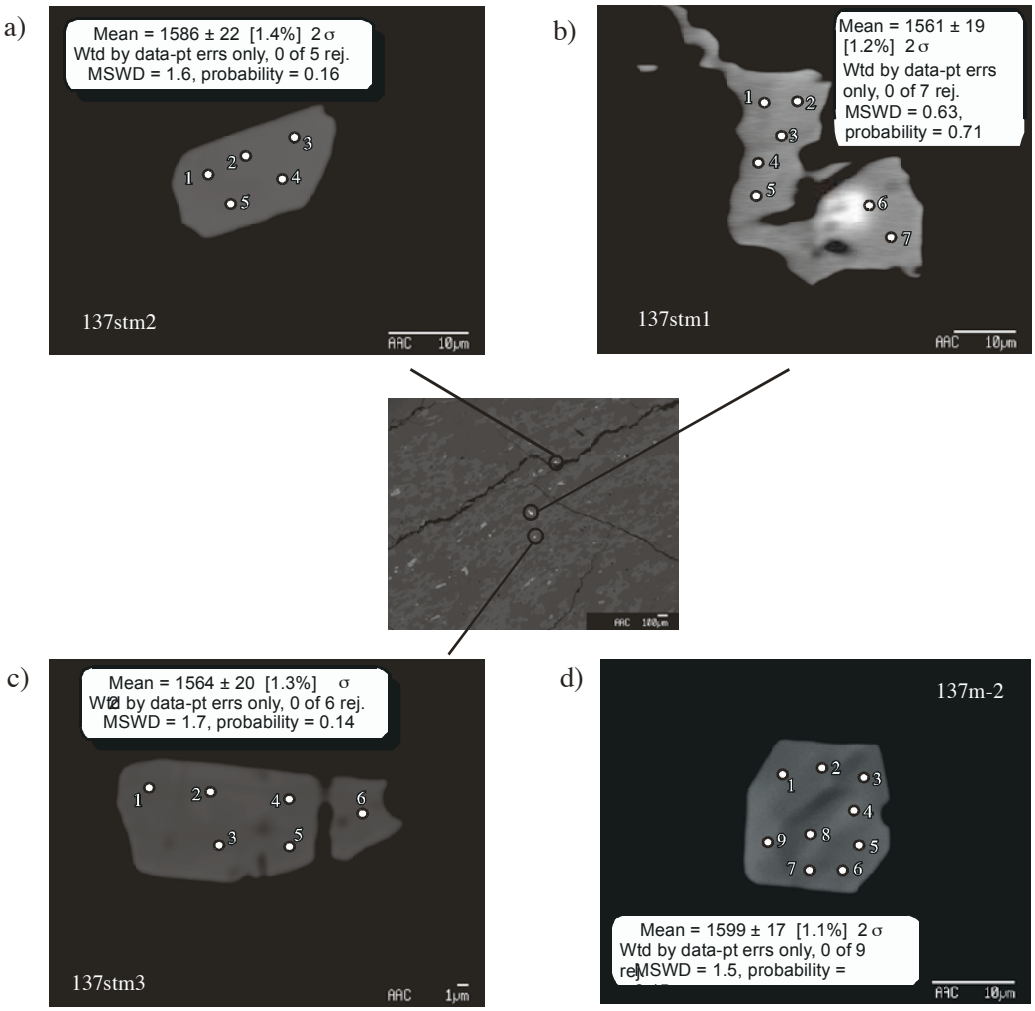
a)
Mean = 1586 ± 22 [1.4%] 2σ
Wtd by data-pt errs only, 0 of 5 rej.
MSWD = 1.6, probability = 0.16
137stm2
b)
Mean = 1561 ± 19
[1.2%] 2σ
Wtd by data-pt errs
only, 0 of 7 rej.
MSWD = 0.63,
probability = 0.71
137stm1
c)
Mean = 1564 ± 20 [1.3%] σ
Wtd by data-pt errs only, 0 of 6 rej.
MSWD = 1.7, probability = 0.14
137stm3
d)
137m-2
Mean = 1599 ± 17 [1.1%] 2σ
Wtd by data-pt errs only, 0 of 9
rej.MSWD = 1.5, probability =

Figure 13. a) Weighted average plot of 7 individual monazite ages with 95% confidence level for rock sample mc137; b) Probability density curve suggests a single age group.

a)

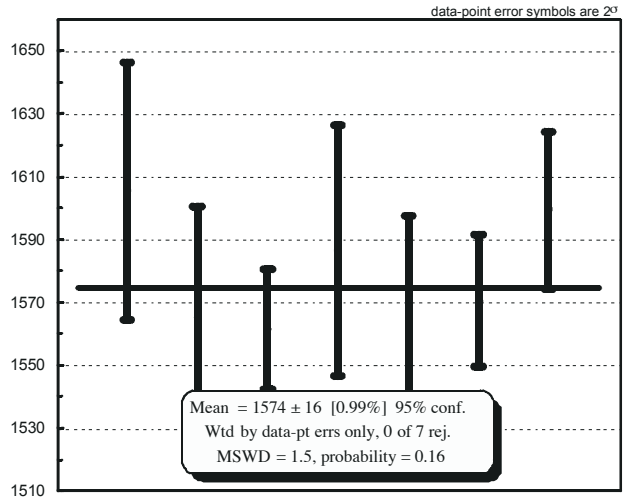

b)

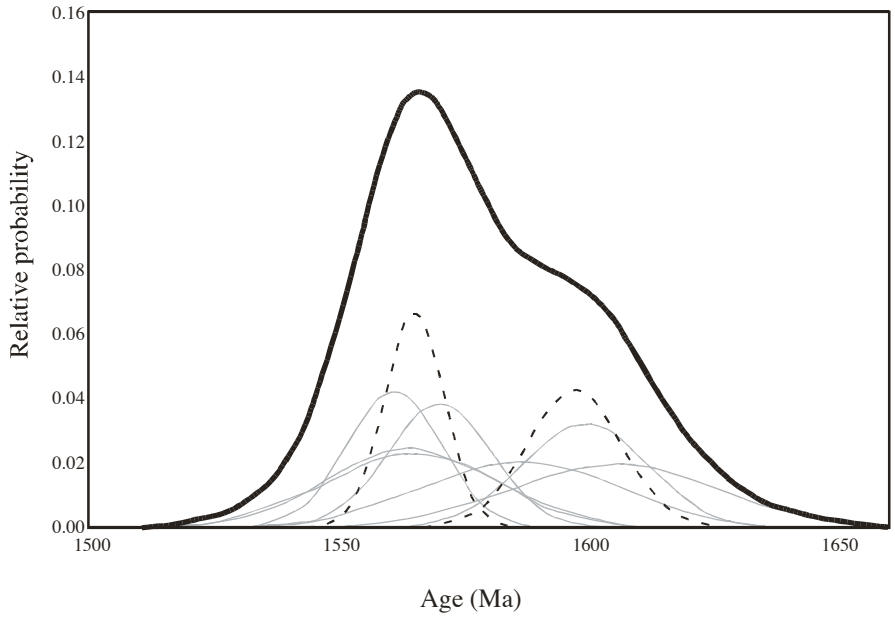

Age	±2 σ	fraction	±2 σ
1567.8	13	0.70	0.69
1596	26	0.30	---

relative misfit = 0.976

Figure 14. Backscatter images show the monazite grains and also their locations (a-b) from sample mc133. The numbered circular spots represent the locations of analyses presented in Table 4.

a)

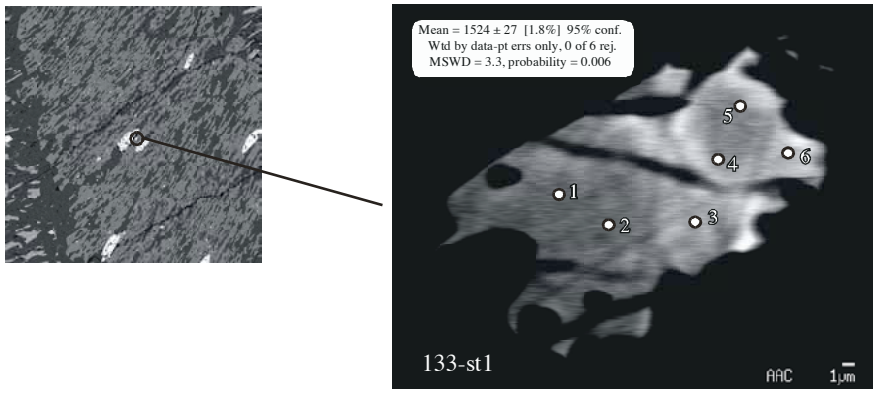
Mean = 1524 ± 27 [1.8%] 95% conf.
Wtd by data-pt errs only, 0 of 6 rej.
MSWD = 3.3, probability = 0.006
1
2
3
4
5
6
133-st1
AAC
1µm

b)

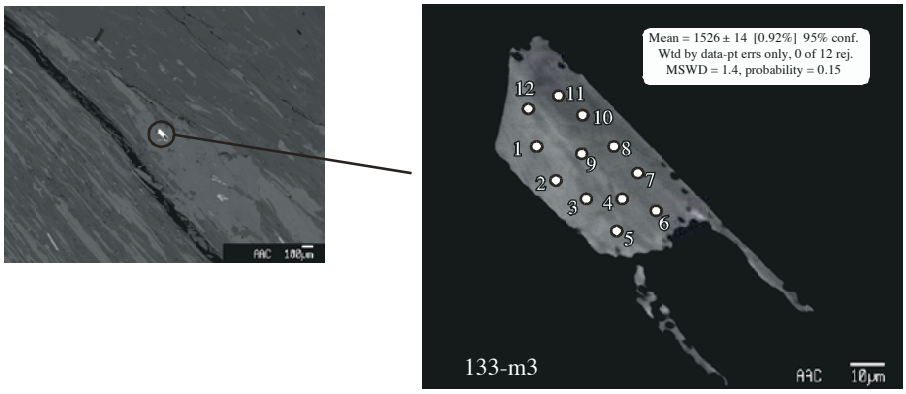
Mean = 1526 ± 14 [0.92%] 95% conf.
Wtd by data-pt errs only, 0 of 12 rej.
MSWD = 1.4, probability = 0.15
1
2
3
4
5
6
7
8
9
10
11
12
133-m3
AAC
10µm

Figure 15. a) Weighted average plot of 5 individual monazite ages with 95% confidence level for rock sample mc133; b) Probability density curve suggests normal distribution of a single age population.

a)

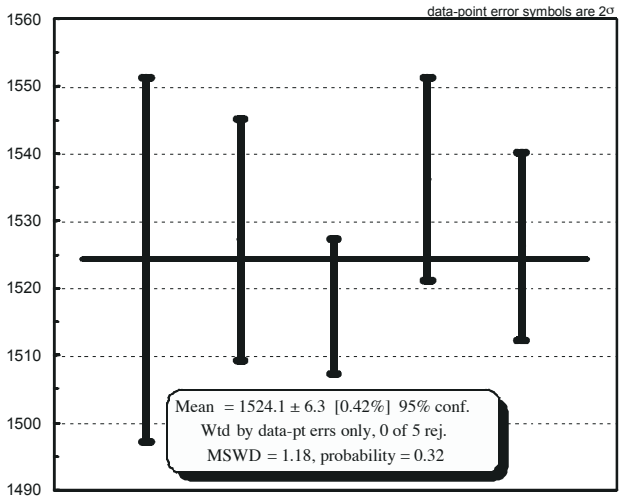

b)

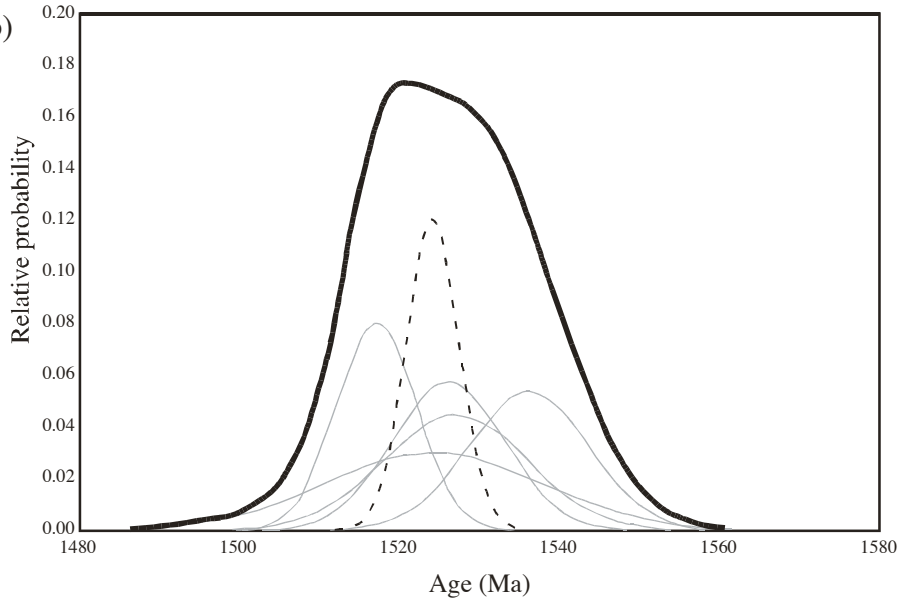

Age	±2 σ	fraction	±2 σ
1520.8	10	0.53	0.86
1529.7	14	0.47	---

relative misfit = 0.991

Figure 16. a) Weighted average plot of 27 individual monazite ages with 95% confidence level from all rock samples; b) Probability density curve suggests three distinct age populations.

a)

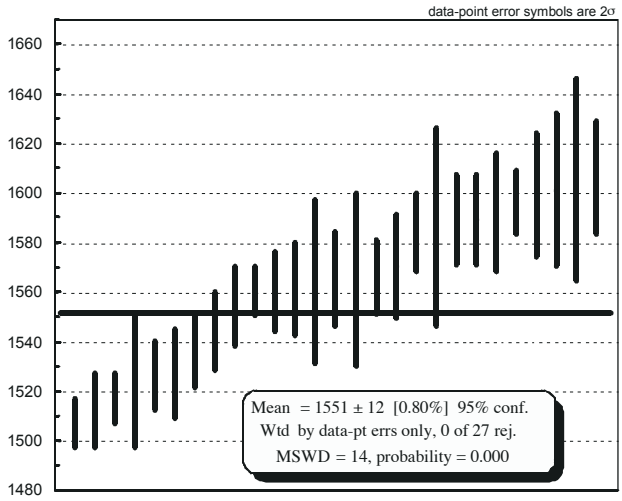

b)

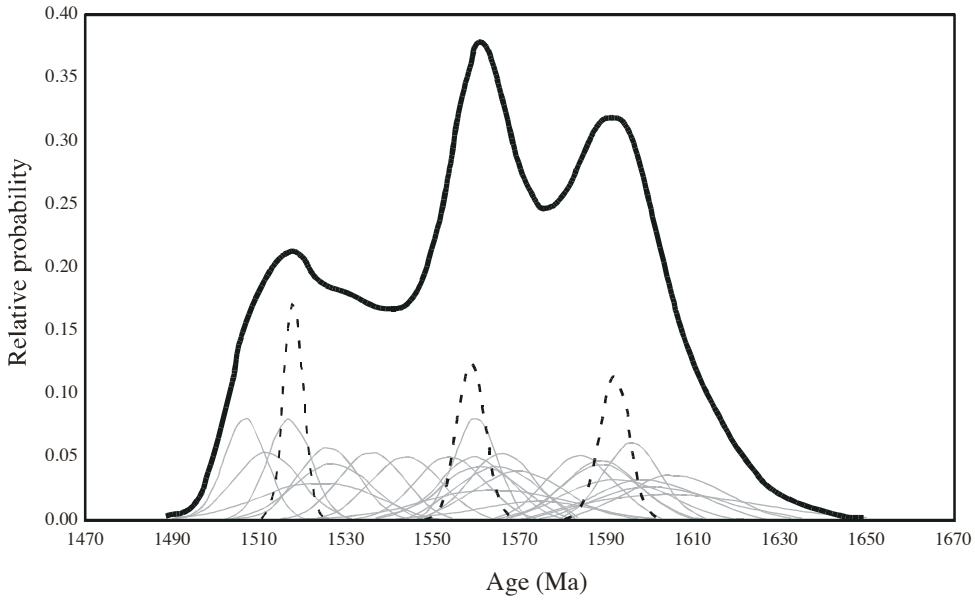

Age	±2 σ	fraction	±2 σ
1518	5.6	0.25	0.20
1559.3	6.3	0.37	0.25
1592.2	6.9	0.38	---

relative misfit = 0.468

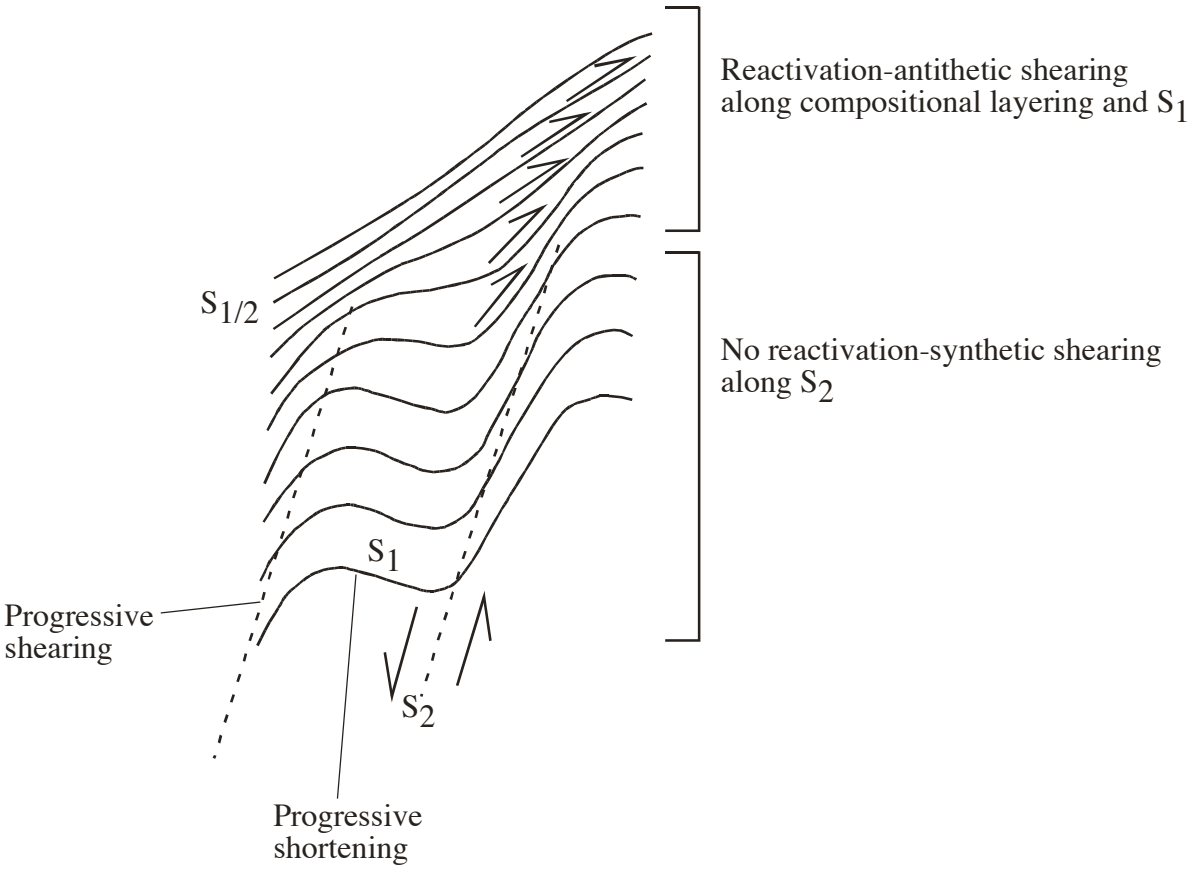

Figure 17. Sketch showing decrenulation of early-formed differentiated crenulation cleavage. Progressive synthetic shearing parallel to S_2 switches to progressive antithetic shearing along S_1-$S_{1/2}$ across a boundary between reactivated and non-reactivated zones; thereby early deformation partitioning domains (progressive shearing and progressive shortening) are locally destroyed.

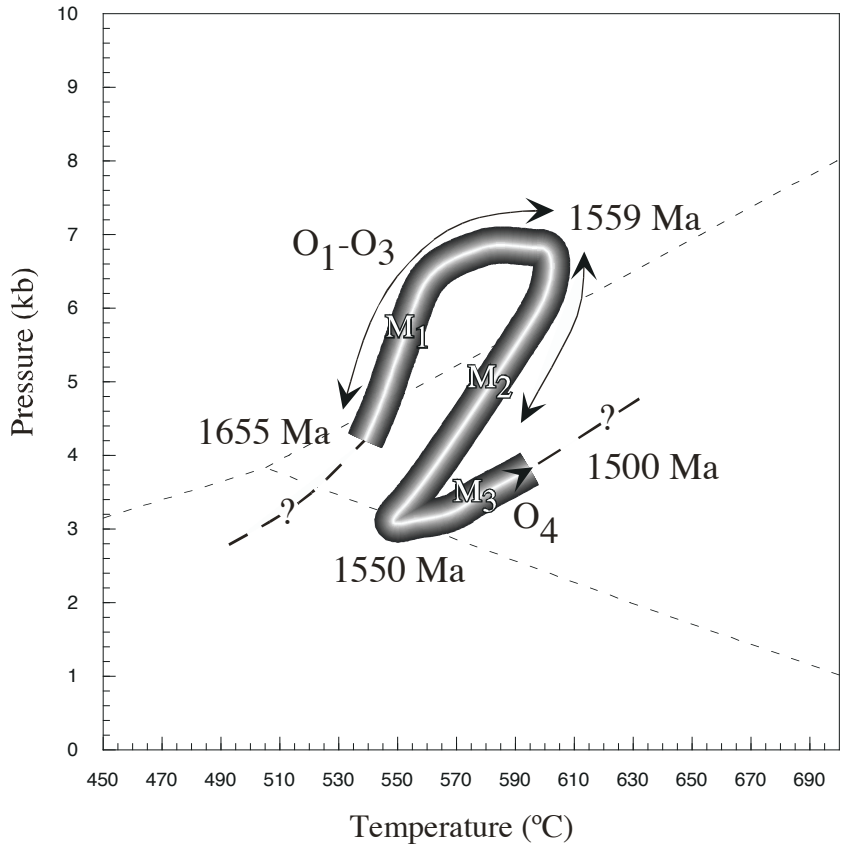

Figure 18. P-T-D-t diagram that shows clockwise loop overprinted by gently sloping path with increasing pressure and temperature. O_1-O_4 stands for deformation periods characterized by NNW-SSE, N-S, E-W and NW-SE, respectively. M_1 represents early medium pressure-temperature metamorphism, followed by retrogressive metamorphism, M_2, which are overprinted by low pressure-high temperature metamorphism, M_3.